Aberystwyth University

Former extent of glacier-like forms on Mars

Link to published article:

This is a manuscript of an article accepted for publication by Elsevier Inc. in Icarus on 11/03/2016, available online: http://dx.doi.org/10.1016/j.icarus.2016.03.006.

Former extent of glacier-like forms on Mars

Stephen BROUGH[a*], Bryn HUBBARD[a] and Alun HUBBARD[a, b]

*a*Department of Geography and Earth Sciences, Aberystwyth University, Ceredigion SY23 3DB, UK

*b*Centre for Arctic Gas Hydrate, Environment and Climate, Department of Geology, University of Tromsø, Tromsø N-9037, Norway

*Corresponding author. Email: stb20@aber.ac.uk

Abstract: Mars' mid-latitude glacier-like forms (GLFs) have undergone substantial mass loss and recession since a hypothesised last martian glacial maximum (LMGM) stand. To date, there is a lack of knowledge of the nature and timing of the LMGM, the subsequent mass loss and whether this mass loss has been spatially variable. Here, we present the results of a population-scale inventory of recessional GLFs, derived from analysis of 1293 GLFs[1] identified within Context Camera (CTX) imagery, to assess the distribution and controls on GLF recession. A total of 436 GLFs were identified showing strong evidence of recession: 197 in the northern hemisphere and 239 in the southern hemisphere. Relative to their parent populations, recessional GLFs are over-represented in the low latitude belts between 25 and 40° and in areas of high relief, suggesting that these zones exert some control over GLF sensitivity and response to forcing. This analysis is complemented by the reconstruction of the maximum extent and morphology of a specific GLF for which High Resolution Imaging Science Experiment (HiRISE) derived digital elevation data are available. Using Nye's (Nye, J. F. [1951] *Proc. Roy. Soc. Lond, Ser. A-Mat. Phys. Sci, 207, 554-572*) perfect plastic approximation of ice flow applied to multiple flow-lines under an optimum yield strength of 22 kPa, we calculate that the reconstructed GLF has lost an area of 6.86 km^2 with a corresponding volume loss of 0.31 km^3 since the LMGM. Assuming the loss reconstructed at this GLF occurred at all mid-latitude GLFs yields a total planetary ice loss from Mars' GLFs of 135 km^3, similar to the current ice volume in the European Alps on Earth.

---

[1] In their inventory Souness et al. (2012) identified 1309 GLFs. We refine the number of GLFs to 1293, due to the identification of duplicate entries.

1. Introduction

Although water ice is not presently stable across much of Mars' mid-latitudes (Mellon and Jakosky, 1995; Mellon et al., 2004), evidence of pervasive ice-rich landforms between 30 and 60° latitude has been presented (Sharp, 1973; Squyres, 1978, 1979; Lucchitta, 1984; Mangold, 2003; Milliken et al., 2003; Levy et al., 2007; Baker et al., 2010; Dickson et al., 2010; Head et al., 2010, Souness et al., 2012; Hubbard et al., 2014; Brough et al., 2016; Sinha and Murty, 2015). Based on evidence from the Shallow Radar (SHARAD) instrument on board the Mars Reconnaissance Orbiter (MRO), the composition of these ice-rich deposits is consistent with water ice (Holt et al., 2008; Plaut et al., 2009), and their surface morphologies are indicative of viscous flow of that ice (e.g. Squyres, 1979; Mangold, 2003; Head et al., 2005). Collectively, these ice-rich deposits have become known as viscous flow features, or VFFs (Milliken et al., 2003), and are hypothesised to have been formed during a previous 'ice age' as a result of changes in orbital and atmospheric parameters providing preferential conditions for mid-latitude ice accumulation during periods of high (>30°) obliquity (Head et al., 2003; Forget et al., 2006; Madeleine et al., 2009; Fassett et al., 2014). The last major change from a high (~35°) to low (~25°) mean obliquity period occurred ~4–6 Ma BP (Laskar et al., 2004), perhaps causing the end of the hypothesised last martian glacial maximum, or LMGM (Souness and Hubbard, 2013). The persistence of VFFs to the present day is therefore probably due, at least partly, to their ubiquitous debris cover protecting the underlying ice from sublimating into the atmosphere (Bryson et al., 2008; Holt et al., 2008; Plaut et al., 2009; Fastook et al., 2014).

Glacier-like forms (GLFs) are a distinctive subtype of VFFs, similar in planform appearance to terrestrial valley glaciers or debris-covered glaciers (e.g. Arfstrom and Hartmann, 2005; Hubbard et al., 2011; Souness et al., 2012). GLFs form in cirque-like alcoves or valleys and appear to flow downslope, generally coalescing from a wide upper basin to a narrow elongate tongue that is often confined by raised latero-terminal ridges. GLFs may or may not feed into pre-existing VFFs and form what Head et al. (2006, 2010) described as Mars' integrated glacial landsystem. Following this model, GLFs represent the smallest component of this glacial landsystem and may converge downslope to form broad, rampart-like lobate debris aprons (LDAs). Where LDAs converge or coalesce, complex and contoured surfaces termed lineated valley fill (LVF) are commonly observed (Squyres, 1978, 1979; Lucchitta, 1984).

3

GLFs and other VFFs (LDA or LVF) have been interpreted as relict remains of once far larger ice masses (Dickson et al., 2008; Sinha and Murty, 2013; Hubbard et al., 2014; Brough et al., 2016), that were most extensive during a hypothesised LMGM (Souness and Hubbard, 2013). For example, in a two-dimensional planform analysis of a GLF in Phlegra Montes, Hubbard et al. (2014) noted a set of pronounced ridges resembling terrestrial moraines, encompassing a texturally distinct 'arcuate' terrain, devoid of many impact craters, in the forefield of a GLF. The contrast between this distinct landform and the wider surface led the authors to suggest that the proglacial arcuate terrain represented a phase of expanded glaciation, and that the GLF had subsequently receded by up to ~3.3 km. Such an expanded former extent has also been identified on GLFs elsewhere on Mars (Hubbard et al., 2011; Hartmann et al., 2014), as well as on the regional scale of Mars' integrated glacial landsystem (e.g. Head et al., 2006; Dickson et al., 2008; Fastook et al., 2014), where surface lowering of up to ~900 m has been inferred (Dickson et al., 2008). Indeed, the identification of relict landforms of glacial origin across large areas of Mars has led to inferences of former regional- to continental-scale ice sheet glaciation (Kargel et al., 1995; Hobley et al., 2014; Souček et al., 2015). Furthermore, several studies have noted the superposed relationship of some GLFs to the underlying ice-rich terrain (LDA or LVF) onto which they appear to have flowed, leading to suggestions of recurrent glacial phases with at least one 'local' glacial phase advancing over an earlier 'regional' glaciation (Levy et al., 2007; Dickson et al., 2008; Baker et al., 2010; Sinha and Murty, 2013; Brough et al., 2016). Despite these inferred changes, we currently have limited knowledge of the nature and timing of Mars' LMGM, the volume of ice lost since that time, and whether such GLF recession has been spatially variable (e.g. Hubbard et al., 2014).

On Earth, the vast majority of valley glaciers have experienced an expanded former extent, or glacial maximum, and have receded since that time (Zemp et al., 2009; Radić and Hock, 2014; Fischer et al., 2015). The visible imprint of such recession, or in some cases complete deglaciation, is recorded to varying degrees in the geomorphic and sedimentary record. Detailed investigation of these remnant landform and sediment assemblages can therefore be used to reconstruct former glacier limits and thermal conditions (e.g. Kleman et al., 1997; Hambrey and Glasser, 2012). Furthermore, due to their short response times, valley glaciers have become important indicators of climatic change (Hambrey

et al., 2005; Raper and Braithwaite, 2009; Carrivick et al., 2015). Thus, if the processes and responses of martian GLFs are broadly equivalent to their terrestrial counterparts, they may represent (i) effective geomorphic agents, through both erosion and deposition, and (ii) important archives of recent climatic change on Mars.

The aim of this paper is to advance our understanding of the glacial history of Mars' GLFs by assessing and quantifying the distribution of, and controls on, GLF recession. Specifically we (i) provide a population-scale inventory detailing the locations of GLFs that show evidence of recession; (ii) analyse the environmental settings of recessional GLFs to assess likely controlling variables on their spatial distribution; and (iii) provide a high-resolution three-dimensional reconstruction of a typical recessional GLF to calculate its volume and area change.

2. Data and methods

2.1. Population-scale recessional GLF inventory

2.1.1. Mapping distribution and morphology

Identification of recessional GLFs was based on analysis of all GLFs in the database of Souness et al. (2012). This database contains the Context Camera (CTX [6 m per pixel]) image ID, coordinate information and basic morphometric and environmental data for all identified GLFs. All GLFs in the database were manually examined by eye using Arizona State University's Mars Image Explorer (http://viewer.mars.asu.edu/) and JMARS software (https://jmars.asu.edu/). GLFs showing evidence of an expanded former extent (Fig. 1) were recorded into a separate database (published as supplementary material to this manuscript) and subsequently imported and plotted, based on the coordinate data of Souness et al. (2012), using ESRI's ArcMap 10.1 Geographic Information System (GIS) software.

2.1.2. Spatial distribution

To determine what, if any, controls are responsible for the observed spatial distribution of recessional GLFs, several environmental parameters were extracted and analysed. These include latitude (^{o}), longitude (^{o}), elevation (m relative to Mars datum), relief (m) and orientation (^{o}). Following Souness et al. (2012) relief was calculated as the standard deviation of elevation values extracted from a 5 km

radius buffer from the GLF's head. As well as plotting recessional GLF counts against these variables, both the recessional GLF population and the total GLF population were normalised against their total counts (436 and 1293, respectively), and the subsequent normalised ratio of recessional GLFs relative to total GLF population plotted to evaluate the relative abundance of recessional GLFs (with a ratio >1 indicating over-representation and <1 indicating under-representation).

The normalised ratio plots for global and hemispheric GLF coverage are presented herein. The global and hemispheric recessional GLF counts can be found in the accompanying supplementary material to this manuscript (Figs. S1–S4).

2.2. Case study: Crater Greg GLF reconstruction

The presence of overlapping High Resolution Imaging Science Experiment (HiRISE) satellite imagery allows high-resolution digital elevation models (DEMs) to be created (e.g. Kirk et al., 2008). Here we utilise a 2 m per pixel DEM (stereo pair PSP_002320_1415_RED and PSP_003243_1415_RED [see Hubbard et al., 2011 for details]) and corresponding orthorectified HiRISE image, with a resolution of ~0.25 m per pixel, to reconstruct the former extent of a well-studied GLF (e.g. Hartmann et al., 2003; Marchant and Head, 2003; Milliken et al., 2003; Kargel, 2004; Hubbard et al., 2011 [Fig. 2d]).

2.2.1. Study site

Our case study reconstruction is based on the analysis of a GLF located in Crater Greg, eastern Hellas Planitia (Fig. 2). This crater is located in a climatically important zone with global climate models suggesting that it was positioned in one of two regions of high ice deposition outside of the polar ice-caps during periods of high obliquity (Forget et al., 2006; Hartmann et al., 2014).

Several lobate tongues classified as GLFs are located on the northern wall of Crater Greg (Arfstrom and Hartmann, 2005; Hubbard et al., 2011; Souness et al., 2012; Hartmann et al., 2014 [Fig. 2c]). The GLF studied herein (Fig. 2d), is ~4 km long and ~1–2 km wide, extends down-slope at an angle of ~10°, and according to Hartmann et al. (2014) is likely younger than ~50 Ma BP, with a best estimate of ~2–9 Ma BP. Several arcuate ridges visible in the immediate forefield of the GLF (Fig. 2d) have been interpreted as latero-terminal moraines (Hubbard et al., 2011; Hartmann et al., 2014) – a type of

moraine that demarcates not only the frontal position of an ice mass but also provides geometric

constraints on former lateral and vertical extents, an important component of glacier reconstruction on

Earth (e.g. Benn et al. 2005). Based on the GLF's overall geomorphological characteristics, Hubbard

et al. (2011) concluded that the upper basin currently hosts a degraded GLF, while the lower basin

zone represents deglaciated terrain.

Although several authors have commented on the degraded nature of this GLF, with previous

estimates of thinning based on heights of the innermost set of lateral moraines of between 30 and 50

m (Hubbard et al., 2011; Hartmann et al., 2014), no attempt has been made to reconstruct the GLF's

former three-dimensional extent, or to quantify the volume of ice lost since that maximum extent.

2.2.2. Glacial reconstruction

In order to assess changes in volume and area of our selected GLF we use standard GIS routines in

ESRI's ArcMap v10.1 (e.g. Wolff et al., 2013). Below, we detail the methods used to reconstruct the

GLFs paleo-ice surface and to calculate morphometric change since the time of that extent. We

summarise sources of potential uncertainty that may arise during our reconstruction in Section 2.3.

The outlines of the current and former GLF surface were manually digitised on screen. The former

GLF outline was mapped on the basis of clear moraine ridges (Section 2.2.1) and associated

geomorphological evidence such as the locations of trimlines (Fig. 3). To demarcate the current GLF

surface we follow the interpretation of Hubbard et al. (2011) to isolate the surface with a relatively

fresh, sharp appearance (including their 'scaly' and 'polygonized' terrains). These terrains contrast

sharply with the surrounding material, which is dominated by heavily dissected unconsolidated

material to the north (termed 'incised-headwall' terrain by Hubbard et al. [2011]; Fig. 3b), and regions

of round to elongate ridges to the south (their 'mound-and-tail' and 'linear' terrain; Fig. 3c). These

outer terrains were interpreted by Hubbard et al. (2011) as consistent with regions of former

glaciation.

In order to recreate the former GLF's bed, we removed the later set of moraine ridges located between the current and former GLF surfaces by clipping them from the DEM and re-interpolating the surface using ArcMap's 'Topo to Raster' (ANUDEM algorithm) tool.

To reconstruct the paleo-ice surface, we calculated the ice thickness along an array of 17 flow-line profiles that extend from the terminus of the outer moraine ridge up to the GLF's headwall. Flow-lines were created based on geometric considerations of terrestrial glacier flow. Each flow-line was converted into a series of nodes at 100 m intervals (Fig. 3a) and, following Van der Veen's (1999, pg 149 – EQ. 6.2.3) adaptation of Nye's (1951, 1952) perfect-plasticity approximation for ice flow, the GLF surface elevation was solved at each node from the margin iterating up-glacier to the headwall. The perfect-plasticity approximation assumes that ice deforms at an infinite rate when the driving stress exceeds a critical yield strength (Van der Veen, 1999). Yield strength values for terrestrial glaciers typically range from 50–150 kPa (Cuffey and Paterson, 2010). However, recent SHARAD-validated measurements of ice thickness on Mars using the same perfect-plastic approach utilised herein, reveal a critical yield strength value of 22 kPa (Karlsson et al., 2015); a value markedly lower than those derived for terrestrial glaciers due, potentially, to the impurity content of martian ice, which is estimated to be between 5 % and 10 % (Holt et al., 2008; Grima et al., 2009; Karlsson et al., 2015). For our GLF reconstruction we adopted this yield strength value bracketed by two additional scenarios to reflect low (12 kPa) and high (38 kPa) yield strengths (Karlsson et al., 2015). Calculation of driving stress followed Van der Veen (1999) and accordingly uses a lower gravitational constant of 3.71 m s^{-2} for Mars compared to Earth. To constrain the zero thickness boundary around the reconstructed GLF, we converted the mapped former margin to nodes at 50 m intervals and extracted the elevation from the HiRISE DEM (Fig. 3a). Finally, by combining these values, the former GLF's paleo-ice surface was interpolated using ArcMap's 'Topo to Raster' tool, which has previously provided robust results for glacier surface interpolation (e.g. Racoviteanu et al., 2007; Carrivick et al., 2015). Our reconstructed GLFs were generated at a resolution of 2 m per pixel to allow direct comparison with the original DEM. We estimated the GLF's former ice thickness by subtracting the GLF's current DEM (with the inner moraines removed) from each of the three reconstructed surfaces. Volume and area change was calculated using Arc Map's 'cut and fill' tool.

2.3. Uncertainty in recession identification and reconstruction

Both the identification of recession and the GLF reconstruction used herein are subject to uncertainties, some of which are constrained and others are not. Below we summarise the sources of these uncertainties and outline their management.

2.3.1. Identification of recession

As with all remotely sensed manual classification studies, there is a potential degree of human error, mainly reflecting the user's ability to identify their features of interest (Smith, 2011). However, evidence of GLF recession was considered to be unambiguous, with geometric changes visible in clearly identifiable latero-terminal moraine ridges and/or in clear surface depressions. Further, the identification of recession depends on the production and subsequent survival of evidence until the time of image acquisition, while any feature must be greater than the observable resolution of the imaging sensor (Smith, 2011).

2.3.2. Identification and digitisation of GLF extent

In the absence of field validation, demarcating the current and former limit of a GLF is solely based on geomorphological and surface features identified in satellite imagery. The identification of glacier boundaries, particularly exemplified on debris covered glaciers, is inherently difficult in remotely-sensed imagery and subject to variable observer interpretation (e.g. Nuimura et al., 2015). Although mitigated by the high resolution of the satellite imagery and DEM used, defining exact boundaries involves some error.

2.3.3. Removal of moraine ridges

Care was taken to remove only the proportion of the surface affected by the inner set of moraine ridges, rather than any natural surface perturbation. This is effectively mitigated because moraine ridges were easily identifiable in contours where they appear as sharp crested peaks.

2.3.4. Creation of DEMs

The choice of interpolation routine causes variation in the reconstructed surface depending on the method used (e.g. inverse distance weighting, spline, kriging, tin). We use the Topo to Raster

interpolation method as it has been shown to produce improved results relative to other interpolation methods (Racoviteanu et al., 2007), and has previously provided reliable estimates of former ice surfaces (Racoviteanu et al., 2007; Carrivick et al., 2015). Although the choice of pixel size used in interpolation is user-defined, it has previously been shown to have a negligible influence on volume calculations (e.g. Villa et al., 2007).

2.3.5. Surface reconstruction and change analysis

In the absence of SHARAD-validating measurements, we do not remove the current GLF volume or potential proglacial sediment in-fill from our DEM. However, under the GLF's current degraded state, it is unlikely that either of these materials is greater than metres to tens of metres thick (Hubbard et al., 2011). We therefore assume the present valley floor, with the innermost moraine ridges removed (Sections 2.2.2 & 2.3.3), represented the former GLF bed for our reconstruction scenarios.

3. Results

3.1. Population-scale distribution of recessional GLFs

From a total population of 1293 GLFs located in Mars' mid-latitudes, 436 (33.7 %) show evidence of an expanded former extent (Fig. 4). Of these 436 recessional GLFs, 197 (45.2 %) are located in the northern hemisphere, and 239 (54.8 %) in the southern hemisphere. Several clusters of recessional GLFs are visible, e.g., across the 'fretted terrain' of the northern dichotomy boundary and surrounding the Hellas impact basin (Fig. 4). This distribution broadly reflects concentration variations in the parent population, resulting in recessional:total GLF ratios close to 1 (Fig. 4).

3.2. Environmental controls over recessional GLF distribution

3.2.1. Latitude

The latitudinal distribution of recessional GLFs shows inter-hemispheric similarity, with a mean of 38.4° in the northern hemisphere and 39.0° in the southern hemisphere (Table 1). However, in both hemispheres, the lower-latitude regions between ~25 and 40° are over-represented by recessional GLFs, with a mean ratio of 1.33, relative to the regions between 40 and 65°, where a mean (under-represented) ratio of 0.64 is observed (Fig. 5a). This effect strengthens at even lower latitudes within

the surveyed region, such that the mean ratio rises to 1.83 between 28 and 32° in the northern hemisphere and to 1.72 between 26 and 30° in the southern hemisphere (Fig. 5a).

3.2.2. Elevation

In contrast to latitudinal distribution of recessional GLFs, there are distinct inter-hemispheric differences in terms of elevation. Mean recessional GLF elevation of the northern and southern hemispheres was -1170 and (+)900 m (Table 1) respectively. In the northern hemisphere, recessional GLFs appear over-represented (ratio up to 2) at elevations close to 0 m, particularly between -500 and (+)2000 m (Fig. 5c). In the southern hemisphere, apart from one isolated peak between -6500 and -6000 m (ratio ~2.5) and some minor fluctuations between -2000 and (+)7500 m, the elevation of recessional GLFs appears to generally reflect that of the parent GLF population (e.g. ratio of ~1).

3.2.3. Relief

The relief of recessional GLFs generally shows that they are over-represented towards the higher relief index values between 700 and 1000 m (Fig. 5e–g). The mean relief index of recessional GLFs has a value of 340 m (standard deviation = 158 m) in the northern hemisphere and a slightly higher value of 439 m (standard deviation = 178 m) in the southern hemisphere (Table 1).

3.2.4. Orientation

Overall, recessional GLFs are over-represented in a broadly southward-facing orientation range between ~120 and 290° (Fig. 5h). However, this general pattern masks an inter-hemispheric contrast: the mean bearing of recessional GLFs is 49° in the northern hemisphere, with little preference for orientation (Fig. 5i), compared to the southern hemisphere where there is a mean bearing of 175°, and a pronounced southerly (i.e. pole-facing) orientation bias of between 150 and 225° (Fig. 5j, Table 1).

3.3. Case study: Crater Greg GLF reconstruction

The reconstructed GLF's plan-form geometry was larger in all directions than its present day configuration. Overall, the reconstructed GLF appears to have coalesced from a wide upper basin down through a bedrock confined channel, which coupled with two lower alcoves provided mass to

11

the narrow GLF terminus (Figs. 3 and 6). The current GLF has a maximum length and width of 2.3 and 2.5 km respectively, and covers an area of 2.81 km^2. The reconstructed GLF extended ~2.5 km southward down the wall of Crater Greg to the lowest moraine ridge and northward up the steep headwall by ~400–500 m (Fig. 3). The reconstructed GLF's lateral margins extended by ~700 m to the east and ~500 m to the west of the current GLFs margins (Fig. 3). These geometric changes result in the reconstructed GLF having a maximum length and width of 5.2 and 3.5 km respectively, and covering an area of 9.67 km^2. The GLF has therefore experienced a reduction in area of 6.86 km^2, or ~70 %, since its maximum extent.

For each of the three reconstruction scenarios (Fig. 6) we calculated the former GLF's maximum and average ice thickness (Fig. 7), and ice volume loss relative to the present day surface. For our low (12 kPa), mean (22 kPa) and high (38 kPa) yield strength scenarios we calculate: (i) maximum ice thickness as 38, 62, and 97 m; (ii) mean ice thickness as 19, 32, and 54 m; and (iii) ice volume loss as 0.18, 0.31, and 0.52 km^3 respectively. In general, an increase in yield strength equated to an increase in mean and maximum ice thickness, and ice volume loss, such that all values for the high yield strength reconstruction were ~2.5 times greater than the low yield strength reconstruction.

4. Interpretation and discussion

4.1. Controls on GLF recession

One third of all GLFs showed evidence of recession. Such recession appears widespread in both the northern and southern hemispheres (Fig. 4) and covers all latitude, elevation, relief and orientation ranges (Fig. 5). This widespread evidence of recession is therefore indicative of global rather than regional or hemispheric changes in controlling, likely climatic, conditions. On Earth, the locality and survival of glaciers are a result of the interplay of effective precipitation, temperature and topography (Cuffey and Paterson, 2010). These three factors are in turn governed by variation in latitude and altitude on the macro-scale and orientation, relief and distance from a precipitation source at a regional or more local scale.

Latitude and relief appear to exert a systematic control on where recessional GLFs occur on Mars. Both of these environmental parameters show statistical over-representation of recessional GLFs

towards the boundary of their environmental ranges (Fig.5), although it should be noted that total numbers of GLFs are lower in these regions than towards the centre of the ranges (Figs. S2 and S4 in supplementary material).

In terms of latitude, recessional GLFs are over-represented relative to the total GLF population at lower latitudes (i.e. closer to the equator). This over-representation occurs within the latitudinal range between 25 and 40° in both the northern and southern hemisphere and was particularly enhanced between 26 and 32° in both (Fig. 5a). This association was not apparent for the higher pole-ward latitudes between 40 and 65°, where recessional GLFs are conversely equally- or under-represented (Fig. 5a). The over-representation of recessional GLFs in the lower latitudinal domain may be a direct reflection of the current stability of shallow ground ice on the planet. At present, ground ice is suggested to be stable at depths of less than 5 m pole-ward of ~45° (Mellon et al., 2004; Bryne et al., 2009; Schorghofer and Forget, 2012). This limit provides an effective threshold such that near surface ice at lower latitudes is at best meta-stable and susceptible to sublimation/ablation. Thus, although recession is identified across all latitudes, over-representation of recessional GLFs at lower latitudes (25–40° in particular) suggests that ice is being preferentially removed from these localities, with corresponding implications for preferential GLF recession.

In terms of relief, recessional GLFs were over-represented in areas of higher relief index values in both the northern and southern hemispheres (Fig. 5e–g), albeit covering a slightly lower index value in the northern hemisphere (550–800 m) than in the southern hemisphere (700–1000 m) (Fig. 5e–g). This hemispheric difference mirrors that of the overall GLF population (Souness et al., 2012 [Figs. S2 and S4 in supplementary material]), and also potentially that identified at the wider VFF scale (e.g. Karlsson et al., 2015). On Earth, relief plays an important role in glacier formation and preservation. On higher relief (steeper) slopes, glaciers are prone to particularly rapid mass change due to a high sensitivity to changes in mass balance and potentially increased solar insolation if they are tilted towards the Sun (see discussion below), or even complete mass loss as a result of avalanching (e.g. Raper and Braithwaite, 2009). While there is little evidence of ice avalanching on Mars, steeper GLFs are still likely to respond more rapidly to climatic change. Although recession is observed across all relief values, the over-representation of recessional GLFs at higher relief values may therefore reflect

13

that they have already re-adjusted their mass distribution to recent climatic change(s), whereas lower relief GLFs are still re-adjusting to climatic perturbations. Furthermore, surface debris can accumulate to thicker depths on shallower slopes, a process that would further dampen the rate in mass response of lower-relief GLFs (e.g. Marchant et al., 2002).

The over-represented recessional GLF latitude and relief domains often host low total GLF numbers (Souness et al., 2012 [Figs. S2 and S4 in supplementary material]). We attribute this association to environmental conditions that are marginal for initial GLF formation, and/or their subsequent preservation.

In terms of elevation and orientation, there was no clear systematic pattern of recessional GLFs visible at either the global or hemispheric scale. For example, Souness et al. (2012) found that GLFs showed a strong pole-ward bias in orientation in both the northern and southern hemisphere. These authors related this bias to the fact that pole-facing alcoves received lower insolation than equatorial facing alcoves and therefore, much like terrestrial glaciers, were more likely to be conducive to accumulation and preservation of ice. Thus, if orientation was to exert a dominant control over GLF recession, one would expect to see GLFs facing away from their nearest pole (i.e. equatorial facing: south in the northern hemisphere and north in the southern hemisphere) to be over-represented – a pattern that was not identified (Fig. 5h–j).

There are at least two potential explanations as to why no orientation bias was observed in the distribution of recessional GLFs. First, this inventory only considers current GLFs and does not consider potential sites of former GLFs that have been either partially removed (e.g. Fig. 1d), and therefore no longer conform to the definition of a GLF as set out by Souness et al. (2012), or completely removed so that a glaciated (ice free) landscape now prevails (e.g. Fig. 1d). During lower obliquity periods, equator-facing slopes are likely to receive higher insolation than pole-facing slopes, and equator-facing GLFs are therefore more likely to be preferentially removed than pole-facing GLFs. Second, it may be possible that a regime similar to those used to explain scalloped terrain development (e.g. Lefort et al., 2009; Ulrich et al., 2010; Séjourné et al., 2011) and gully formation (Costard et al., 2002) may also affect GLFs. Here, it is argued that during periods of very high

obliquity (≥45°) pole-facing slopes become the more likely regions of higher insolation and day-averaged summer temperatures, and thus preferential sites for ice removal, relative to equator-facing slopes (Costard et al., 2002). If we take into account obliquity variation over the last 20 Ma, a period for which reliable obliquity solutions have been obtained (Laskar et al., 2004) and one which covers the possible age of GLFs (Hartmann et al., 2014), Mars has experienced at least six periods of obliquity of ≥45° (Laskar et al., 2004). However, it should be noted that these high obliquity excursions are relatively short lived and that the last 20 Ma has been dominated by obliquity ≤45° (Laskar et al., 2004). Therefore, it is possible that at least two contrasting signals are manifested in the orientation distribution of recessional GLFs, with one preferentially reducing/removing equator-facing GLFs and the other preferentially reducing/removing pole-facing GLFs. Although the exact contribution and importance of these processes to ice removal remains unknown, it does provide a potential explanation for the observed orientation distribution of recessional GLFs.

Taken together, these results can add further perspective to the development and evolution of glacial/periglacial landforms in Mars' mid-latitudes. Several landforms or terrains, including dissected mantle terrain (Mustard et al., 2001; Kreslavsky and Head, 2002; Milliken and Mustard, 2003), banded terrain (Diot et al., 2014), scalloped depressions (Lefort et al., 2009; Ulrich et al., 2010; Séjourné et al., 2011), polygons (Mangold, 2005), and VFFs (Milliken et al., 2003; Souness et al., 2012; Levy et al., 2014) appear between 30 and 60° in both hemispheres, and have been, to various degrees, attributed to latitude-dependent insolation forcing. The identification of a latitudinal threshold at ~40° in both hemispheres, below which GLFs are preferentially removed (Fig. 5), would conform to this hypothesis, particularly as this latitude falls close to the current stability of shallow ground ice on the planet (Mellon et al., 2004; Bryne et al., 2009; Schorghofer and Forget, 2012). However, there is also some degree of heterogeneity in recession, whereby GLFs in a similar setting do not show a similar response (Figs. 4 and 5). It is therefore likely that regional or local meteorological conditions also play a role in GLF survival and/or initial emplacement, as may be the scenario for other mid-latitude glacial/periglacial landforms (Conway and Balme, 2013; Levy et al., 2014).

4.2. Crater Greg GLF reconstruction and population ice loss potential

Our reconstructed GLF in Crater Greg has changed substantially since its former maximum. The GLF has receded 3 km, or ~60 %, of its maximum length, and lost an area of 6.86 km^2, or ~70 %, of its maximum extent (Figs. 6 and 7). Assuming that the mean yield strength of 22 kPa (Section 2.2.2) is the most appropriate value for our GLF reconstruction, we calculate that the GLF had a maximum and mean ice thickness of 62 and 32 m respectively (Fig. 7), and has lost an ice volume of 0.31 km^3. The GLF in Crater Greg has therefore undergone substantial mass loss since the LMGM, with these changes manifested in both surface lowering and terminus recession.

The identification of over 400 GLFs showing evidence of recession, coupled with substantial mass and area loss for our reconstructed case study GLF, suggests that a large proportion of ice has been removed from GLFs since the LMGM. Although tentative, assuming that the volume loss of 0.18-0.52 km^3 from the reconstructed Crater Greg GLF (Section 3.3) is typical of all recessional GLFs (n = 436), yields a first-order estimate of global ice volume loss from GLFs since the LMGM of between 78 and 227 km^3, with a best estimate of 135 km^3 for an optimum yield strength of 22 kPa – an equivalent ice volume to that currently stored in the Alpine glaciers of central Europe (Huss and Farinotti, 2012), although the mass balance terms are likely very different in the two settings.

This generalised estimate does emphasise the requirement for regional- or population-scale reconstruction studies if we are to improve our current understanding of the evolution of mid-latitude ice deposits under a changing martian climate. For example, recessional GLFs in the northern hemisphere have an overall lower elevation and relief index than those in the southern hemisphere (Section 3.2 and Fig. S4 in supplementary material). Thus, these spatially varying conditions, coupled with potential endogenic environmental variability in, for example, ice-debris content, ice grain size or supra-glacial debris layer thickness, are likely to exert some control over the rates of individual GLF recession and volume loss (i.e. a non-uniform recession rate and ice volume change in GLFs [Parsons et al., 2011]) – a ubiquitous occurrence on terrestrial glaciers (e.g. Scherler et al., 2011). Such variability would be captured by high-resolution mapping and reconstruction of all recessional GLFs. Similar studies have proven useful on terrestrial glaciers (e.g. Glasser et al., 2011), and would be a beneficial avenue for future research on Mars.

Several lines of evidence have been presented for partial to complete degradation of non-polar ice deposits (e.g. Head and Marchant, 2003; Dickson et al., 2008; Hauber et al., 2008), and although not formally analysed herein, several instances of alcoves adjacent to GLFs containing ice remnants were observed (e.g. Fig. 1d). It is possible that such deposits are the remains of former GLFs that have partially, or completely, receded since ice emplacement. Thus, in restricting this analysis to identified GLFs (Souness et al., 2012), total ice volume loss has likely been underestimated. Therefore, due to the potential sources of over- or under-estimation outlined above, the estimate of ice volume loss from GLFs reported here should be viewed only as an initial approximation, pending refinement based on a more granular-level analysis.

The estimated ice volume loss from GLFs (135 km^3) is minor relative to the volume of ice contained in the Northern Polar Layered Deposits (~821,000 km^3 [Putzig et al., 2009]), which potentially serves as a likely reservoir exchanging mass with the mid-latitudes (e.g. Head et al., 2003, Levrard et al., 2004). Thus, although not a significant mass exchange at the planetary level, the GLF ice loss we report is potentially important for mid-latitude environmental conditions and landform development.

5. Conclusions

Visual analysis of 1293 GLFs reveals that 436 show evidence of an expanded former extent. This recession is distributed across both the northern and southern hemispheres, thereby indicating widespread climatic change on Mars. Although recession is observed across all environmental parameters, the statistical over-representation of recessional GLFs is particularly pronounced in (i) low latitude and (ii) high relief domains, suggesting that these parameters exert some control over GLF recession. With respect to latitude, GLFs between 25 and 40° in both hemispheres appear to be preferentially experiencing mass loss. Here, the higher latitudinal boundary coincides with the limit of present day ground ice stability, and, as such, may represent a threshold between the effective preservation and sublimation/ablation of GLFs. The over-representation of recessional GLFs in regions of higher relief would suggest that, like their terrestrial counterparts, these ice masses have a shorter response time to climatic perturbations than lower relief GLFs, reflecting the influence of slope on mass redistribution both directly and indirectly via the stability of supraglacial debris. These two domains of over-representation of recessional GLFs are characterised by low total GLF numbers,

suggesting that the areas already represent zones of marginal glaciation, which have subsequently become un-stable under martian climatic change.

Our GLF reconstruction provides, to our knowledge, the first estimate of both area and volume loss from a GLF (noting that similar studies have previously been applied to other, often large scale, ice masses [e.g. Shean et al., 2005]). Results indicate that the case study Crater Greg GLF has receded in area by ~70 % and has lost an ice volume between 0.18 and 0.52 km^3, with a best estimate of 0.31 km^3, since its former maximum extent. Scaling this up to all recessional GLFs ($n = 436$) suggests a global first-order estimate of ice volume loss from Mars' mid-latitude GLFs of between 78 and 227 km^3, with a best estimate of 135 km^3. Future research should focus on refining this estimate through consideration of volume change at all individual recessional GLFs, as well as on the much wider VFF scale (e.g. Levy et al., 2014).

Acknowledgements

Supplementary materials

References

Arfstrom, J., & Hartmann, W. K. (2005). Martian flow features, moraine-like ridges, and gullies: Terrestrial analogs and interrelationships. *Icarus, 174*(2), 321-335. doi: 10.1016/j.icarus.2004.05.026.

Baker, D. M. H., Head, J. W., & Marchant, D. R. (2010). Flow patterns of lobate debris aprons and lineated valley fill north of Ismeniae Fossae, Mars: Evidence for extensive mid-latitude glaciation in the Late Amazonian. *Icarus, 207*(1), 186-209. doi: 10.1016/j.icarus.2009.11.017.

Benn, D. I., Owen, L. A., Osmaston, H. A., Seltzer, G. O., Porter, S. C., & Mark, B. (2005). Reconstruction of equilibrium-line altitudes for tropical and sub-tropical glaciers. *Quaternary International, 138-139*, 8-21. doi: 10.1016/j.quaint.2005.02.003.

Brough, S., Hubbard, B., Souness, C. J., Grindrod, P. M., & Davis, J. (2016). Landscapes of polyphase glaciation: eastern Hellas Planitia, Mars. *Journal of Maps, 12*(3), 530-542. doi: 10.1080/17445647.2015.1047907.

Bryson, K., Chevrier, V., Sears, D., & Ulrich, R. (2008). Stability of ice on Mars and the water vapor diurnal cycle: Experimental study of the sublimation of ice through a fine-grained basaltic regolith. *Icarus, 196*(2), 446-458. doi: 10.1016/j.icarus.2008.02.011.

Byrne, S., Dundas, C. M., Kennedy, M. R., Mellon, M. T., McEwen, A. S., Cull, S. C., Dauber, I. J., Shean, D. E., Seelos, K. D., Murchie, S. L., Cantor, B. A., Arvidson, R. E., Edgett, K. S., Reufer, A., Thomas, N., Harrison, T. N., Posiolova, L. V., & Seelos, F. P. (2009). Distribution of mid-latitude ground ice on Mars from new impact craters. *Science, 325*(5948), 1674-1676. doi: 10.1126/science.1175307.

Carrivick, J. L., Berry, K., Geilhausen, M., James, W. H. M., Williams, C., Brown, L. E., Rippin, D. M., & Carver, S. J. (2015). Decadal-scale changes of the Ödenwinkelkees, Central Austria, suggest increasing control of topography and evolution towards steady state. *Geografiska Annaler: Series A, Physical Geography, 97*(3), 543-562. doi: 10.1111/geoa.12100.

Conway, S. J., & Balme, M. R. (2014). Decameter thick remnant glacial ice deposits on Mars. *Geophysical Research Letters, 41*(15), 2014GL060314. doi: 10.1002/2014gl060314.

Costard, F., Forget, F., Mangold, N., & Peulvast, J. P. (2002). Formation of recent Martian debris flows by melting of near-surface ground ice at high obliquity. *Science, 295*(5552), 110-113. doi: 10.1126/science.1066698.

Cuffey, K. M., & Paterson, W. S. B. (2010). *The Physics of Glaciers* (4th ed.). Oxford: Butterworth-Heinemann.

Dickson, J. L., Head, J. W., & Marchant, D. R. (2008). Late Amazonian glaciation at the dichotomy boundary on Mars: Evidence for glacial thickness maxima and multiple glacial phases. *Geology, 36*(5), 411-414. doi: 10.1130/g24382a.1.

Dickson, J. L., Head, J. W., & Marchant, D. R. (2010). Kilometer-thick ice accumulation and glaciation in the northern mid-latitudes of Mars: Evidence for crater-filling events in the Late Amazonian at the Phlegra Montes. *Earth and Planetary Science Letters, 294*(3-4), 332-342. doi: 10.1016/j.epsl.2009.08.031.

Diot, X., El-Maarry, M. R., Schlunegger, F., Norton, K. P., Thomas, N., & Grindrod, P. M. (2014). The geomorphology and morphometry of the banded terrain in Hellas basin, Mars. *Planetary and Space Science, 101*, 118-134. doi: 10.1016/j.pss.2014.06.013.

Fassett, C. I., Levy, J. S., Dickson, J. L., & Head, J. W. (2014). An extended period of episodic northern mid-latitude glaciation on Mars during the Middle to Late Amazonian: Implications for long-term obliquity history. *Geology, 42*(9), 763-766. doi: 10.1130/g35798.1.

Fastook, J. L., Head, J. W., & Marchant, D. R. (2014). Formation of lobate debris aprons on Mars: Assessment of regional ice sheet collapse and debris-cover armoring. *Icarus, 228*, 54-63. doi: 10.1016/j.icarus.2013.09.025.

Fischer, M., Huss, M., & Hoelzle, M. (2015). Surface elevation and mass changes of all Swiss glaciers 1980–2010. *The Cryosphere, 9*(2), 525-540. doi: 10.5194/tc-9-525-2015.

Forget, F., Haberle, R. M., Montmessin, F., Levrard, B., & Heads, J. W. (2006). Formation of glaciers on Mars by atmospheric precipitation at high obliquity. *Science, 311*(5759), 368-371. doi: 10.1126/science.1120335.

Glasser, N. F., Harrison, S., Jansson, K. N., Anderson, K., & Cowley, A. (2011). Global sea-level contribution from the Patagonian Icefields since the Little Ice Age maximum. *Nature Geoscience, 4*(5), 303-307. doi: 10.1038/ngeo1122.

Grima, C., Kofman, W., Mouginot, J., Phillips, R. J., Hérique, A., Biccari, D., Seu, R., & Ccutigni, M. (2009). North polar deposits of Mars: Extreme purity of the water ice. *Geophysical Research Letters, 36*(3), L03203. doi: 10.1029/2008gl036326.

Hambrey, M. J., & Glasser, N. F. (2012). Discriminating glacier thermal and dynamic regimes in the sedimentary record. *Sedimentary Geology, 251–252*, 1-33. doi: 10.1016/j.sedgeo.2012.01.008.

Hambrey, M. J., Murray, T., Glasser, N. F., Hubbard, A., Hubbard, B., Stuart, G., Hansen, S., & Kohler, J. (2005). Structure and changing dynamics of a polythermal valley glacier on a centennial timescale: Midre Lovénbreen, Svalbard. *Journal of Geophysical Research: Earth Surface, 110*(F1), F01006. doi: 10.1029/2004jf000128.

Hartmann, W. K., Thorsteinsson, T., & Sigurdsson, F. (2003). Martian hillside gullies and Icelandic analogs. *Icarus, 162*(2), 259-277. doi: 10.1016/S0019-1035(02)00065-9.

Hartmann, W. K., Ansan, V., Berman, D. C., Mangold, N., & Forget, F. (2014). Comprehensive analysis of glaciated martian crater Greg. *Icarus, 228*, 96-120. doi: 10.1016/j.icarus.2013.09.016.

Hauber, E., van Gasselt, S., Chapman, M. G., & Neukum, G. (2008). Geomorphic evidence for former lobate debris aprons at low latitudes on Mars: Indicators of the Martian paleoclimate. *Journal of Geophysical Research, 113*(E2), E02007. doi: 10.1029/2007je002897.

Head, J. W., & Marchant, D. R. (2003). Cold-based mountain glaciers on Mars: Western Arsia Mons. *Geology, 31*(7), 641. doi: 10.1130/0091-7613(2003)031<0641:cmgomw>2.0.co;2.

Head, J. W., Mustard, J. F., Kreslavsky, M. A., Milliken, R. E., & Marchant, D. R. (2003). Recent ice ages on Mars. *Nature, 426*(6968), 797-802. doi: 10.1038/Nature02114.

Head, J. W., Marchant, D. R., Agnew, M. C., Fassett, C. I., & Kreslavsky, M. A. (2006). Extensive valley glacier deposits in the northern mid-latitudes of Mars: Evidence for Late Amazonian obliquity-driven climate change. Earth and Planetary Science Letters, 241(3-4), 663-671. doi: 10.1016/j.epsl.2005.11.016.

Head, J. W., Marchant, D. R., Dickson, J. L., Kress, A. M., & Baker, D. M. (2010). Northern mid-latitude glaciation in the Late Amazonian period of Mars: Criteria for the recognition of debris-covered glacier and valley glacier landsystem deposits. *Earth and Planetary Science Letters, 294*(3-4), 306-320. doi: 10.1016/j.epsl.2009.06.041.

Head, J. W., Neukum, G., Jaumann, R., Hiesinger, H., Hauber, E., Carr, M., Massson, P., Foing, B., Hoffmann, H., Kreslavsky, M., Werner, S., Milkovich, S., van Gasselt, S., & HRSC Co-Investigator Team. (2005). Tropical to mid-latitude snow and ice accumulation, flow and glaciation on Mars. *Nature, 434*(7031), 346-351. doi: 10.1038/Nature03359.

Hobley, D. E. J., Howard, A. D., & Moore, J. M. (2014). Fresh shallow valleys in the Martian midlatitudes as features formed by meltwater flow beneath ice. *Journal of Geophysical Research-Planets, 119*(1), 128-153. doi: 10.1002/2013je004396.

Holt, J. W., Safaeinili, A., Plaut, J. J., Head, J. W., Phillips, R. J., Seu, R., Kempft, S. D., Choudhary, P., Young, D. A., Putzig, N. E., Biccari, D., & Gim, Y. (2008). Radar Sounding Evidence for Buried Glaciers in the Southern Mid-Latitudes of Mars. *Science, 322*(5905), 1235-1238. doi: 10.1126/science.1164246.

Hubbard, B., Souness, C., & Brough, S. (2014). Glacier-like forms on Mars. *The Cryosphere, 8*(6), 2047-2061. doi: 10.5194/tc-8-2047-2014.

Hubbard, B., Milliken, R. E., Kargel, J. S., Limaye, A., & Souness, C. J. (2011). Geomorphological characterisation and interpretation of a mid-latitude glacier-like form: Hellas Planitia, Mars. *Icarus, 211*(1), 330-346. doi: 10.1016/j.icarus.2010.10.021.

Huss, M., & Farinotti, D. (2012). Distributed ice thickness and volume of all glaciers around the globe. *Journal of Geophysical Research: Earth Surface, 117*(F4), F04010. doi: 10.1029/2012jf002523.

Kargel, J. S. (2004). *Mars - A Warmer, Wetter Planet*. London: Springer-Praxis.

Kargel, J. S., Baker, V. R., Beget, J. E., Lockwood, J. F., Pewe, T. L., Shaw, J. S., & Strom, R. G. (1995). Evidence of Ancient Continental-Glaciation in the Martian Northern Plains. *Journal of Geophysical Research-Planets, 100*(E3), 5351-5368. doi: 10.1029/94je02447.

Karlsson, N. B., Schmidt, L. S., & Hvidberg, C. S. (2015). Volume of Martian midlatitude glaciers from radar observations and ice flow modeling. *Geophysical Research Letters, 42*(8), 2672-2633. doi: 10.1002/2015gl063219.

Kirk, R. L., Howington-Kraus, E., Rosiek, M. R., Anderson, J. A., Archinal, B. A., Becker, K. J., Cook, D. A., Galuszka, D. M., Geissler, P. E., Hare, T. M., Holmberg, I. M., Keszthelyi, L. P., Redding, B. L., Delamere, W. A., Gallagher, D., Chapel, J. D., Eliason, E. M., King, R., & McEwen, A. S. (2008). Ultrahigh resolution topographic mapping of Mars with MRO HiRISE stereo images: Meter-scale

slopes of candidate Phoenix landing sites. *Journal of Geophysical Research, 113*, E00A24. doi: 10.1029/2007je003000.

Kleman, J., Hattestrand, C., Borgstrom, I., & Stroeven, A. (1997). Fennoscandian palaeoglaciology reconstructed using a glacial geological inversion model. *Journal of Glaciology, 43*(144), 283-299.

Kreslavsky, M. A., & Head, J. W. (2002). Mars: Nature and evolution of young latitude-dependent water-ice-rich mantle. *Geophysical Research Letters, 29*(15). doi: 10.1029/2002gl015392.

Laskar, J., Correia, A. C. M., Gastineau, M., Joutel, F., Levrard, B., & Robutel, P. (2004). Long term evolution and chaotic diffusion of the insolation quantities of Mars. *Icarus, 170*(2), 343-364. doi: 10.1016/j.icarus.2004.04.005.

Lefort, A., Russell, P. S., Thomas, N., McEwen, A. S., Dundas, C. M., & Kirk, R. L. (2009). Observations of periglacial landforms in Utopia Planitia with the High Resolution Imaging Science Experiment (HiRISE). *Journal of Geophysical Research: Planets, 114*(E4), E04005. doi: 10.1029/2008je003264.

Levrard, B., Forget, F., Montmessin, F., & Laskar, J. (2004). Recent ice-rich deposits formed at high latitudes on Mars by sublimation of unstable equatorial ice during low obliquity. *Nature, 431*(7012), 1072-1075. doi: 10.1038/nature03055.

Levy, J. S., Head, J. W., & Marchant, D. R. (2007). Lineated valley fill and lobate debris apron stratigraphy in Nilosyrtis Mensae, Mars: Evidence for phases of glacial modification of the dichotomy boundary. *Journal of Geophysical Research, 112*(E8), E08004. doi: 10.1029/2006je002852.

Levy, J. S., Fassett, C. I., Head, J. W., Schwartz, C., & Watters, J. L. (2014). Sequestered glacial ice contribution to the global Martian water budget: Geometric constraints on the volume of remnant, midlatitude debris-covered glaciers. *Journal of Geophysical Research: Planets, 119*(10), 2014JE004685. doi: 10.1002/2014je004685.

Lucchitta, B. K. (1984). Ice and debris in the Fretted Terrain, Mars. *Journal of Geophysical Research: Solid Earth, 89*(S02), B409-B418. doi: 10.1029/JB089iS02p0B409.

Madeleine, J. B., Forget, F., Head, J. W., Levrard, B., Montmessin, F., & Millour, E. (2009). Amazonian northern mid-latitude glaciation on Mars: A proposed climate scenario. *Icarus, 203*(2), 390-405. doi: 10.1016/j.icarus.2009.04.037.

Mangold, N. (2003). Geomorphic analysis of lobate debris aprons on Mars at Mars Orbiter Camera scale: Evidence for ice sublimation initiated by fractures. *Journal of Geophysical Research, 108*(E4), 8021. doi: 10.1029/2002je001885.

Mangold, N. (2005). High latitude patterned grounds on Mars: Classification, distribution and climatic control. *Icarus, 174*(2), 336-359. doi: 10.1016/j.icarus.2004.07.030.

Marchant, D., & Head, J. W. (2003). Tongue-shaped lobes on Mars: Morphology, Nomenclature, and Relation to Rock Glacier Deposits. Abstract #3091, *Sixth International Conference on Mars, July 20-25, Pasadena, California.*

Marchant, D. R., Lewis, A. R., Phillips, W. M., Moore, E. J., Souchez, R. A., Denton, G. H., Sugden, D. E., Potter Jr, N., & Landis, G. P. (2002). Formation of patterned ground and sublimation till over Miocene glacier ice in Beacon Valley, southern Victoria Land, Antarctica. *Geological Society of America Bulletin, 114*(6), 718-730. doi: 10.1130/0016-7606(2002)114<0718:fopgas>2.0.co;2.

Mellon, M. T., & Jakosky, B. M. (1995). The distribution and behavior of Martian ground ice during past and present epochs. *Journal of Geophysical Research: Planets, 100*(E6), 11781-11799. doi: 10.1029/95je01027.

Mellon, M. T., Feldman, W. C., & Prettyman, T. H. (2004). The presence and stability of ground ice in the southern hemisphere of Mars. *Icarus, 169*(2), 324-340. doi: 10.1016/j.icarus.2003.10.022.

Milliken, R. E., & Mustard, J. F. (2003). Erosional morphologies and characteristics of latitude-dependant surface mantles on Mars. Abstract #3240, *Sixth International Conference on Mars, July 20-25, Pasadena, California*.

Milliken, R. E., Mustard, J. F., & Goldsby, D. L. (2003). Viscous flow features on the surface of Mars: Observations from high-resolution Mars Orbiter Camera (MOC) images. *Journal of Geophysical Research-Planets, 108*(E6), 5057. doi: 10.1029/2002je002005.

Mustard, J. F., Cooper, C. D., & Rifkin, M. K. (2001). Evidence for recent climate change on Mars from the identification of youthful near-surface ground ice. *Nature, 412*(6845), 411-414. doi: 10.1038/35086515.

Nuimura, T., Sakai, A., Taniguchi, K., Nagai, H., Lamsal, D., Tsutaki, S., Kozawa, A., Hoshina, Y., Takenaka, S., Omiya, S., Tsunematsu, K., Tshering, P., & Fujita, K. (2015). The GAMDAM glacier inventory: a quality-controlled inventory of Asian glaciers. *The Cryosphere, 9*(3), 849-864. doi: 10.5194/tc-9-849-2015.

Nye, J. F. (1951). The Flow of Glaciers and Ice-Sheets as a Problem in Plasticity. *Proceedings of the Royal Society of London Series a-Mathematical and Physical Sciences, 207*(1091), 554-572. doi: DOI 10.1098/rspa.1951.0140.

Nye, J. F. (1952). A Method of Calculating the Thicknesses of the Ice-Sheets. [10.1038/169529a0]. *Nature, 169*(4300), 529-530. doi: 10.1038/169529a0.

Parsons, R. A., Nimmo, F., & Miyamoto, H. (2011). Constraints on martian lobate debris apron evolution and rheology from numerical modeling of ice flow. *Icarus, 214*(1), 246-257. doi: 10.1016/j.icarus.2011.04.014.

Plaut, J. J., Safaeinili, A., Holt, J. W., Phillips, R. J., Head, J. W., Seu, R., Putzig, N. E., & Frigeri, A. (2009). Radar evidence for ice in lobate debris aprons in the mid-northern latitudes of Mars. *Geophysical Research Letters, 36*(2), L02203. doi: 10.1029/2008gl036379.

Putzig, N. E., Phillips, R. J., Campbell, B. A., Holt, J. W., Plaut, J. J., Carter, L. M., Egan, A. F., Bernardini, F., Safaeinili, A., & Seu, R. (2009). Subsurface structure of Planum Boreum from Mars Reconnaissance Orbiter Shallow Radar soundings. *Icarus, 204*(2), 443-457. doi: 10.1016/j.icarus.2009.07.034.

Racoviteanu, A. E., Manley, W. F., Arnaud, Y., & Williams, M. W. (2007). Evaluating digital elevation models for glaciologic applications: An example from Nevado Coropuna, Peruvian Andes. *Global and Planetary Change, 59*(1–4), 110-125. doi: 10.1016/j.gloplacha.2006.11.036.

Radić, V., & Hock, R. (2014). Glaciers in the Earth's Hydrological Cycle: Assessments of Glacier Mass and Runoff Changes on Global and Regional Scales. *Surveys in Geophysics, 35*(3), 813-837. doi: 10.1007/s10712-013-9262-y.

Raper, S. C. B., & Braithwaite, R. J. (2009). Glacier volume response time and its links to climate and topography based on a conceptual model of glacier hypsometry. *The Cryosphere, 3*(2), 183-194. doi: 10.5194/tc-3-183-2009.

Scherler, D., Bookhagen, B., & Strecker, M. R. (2011). Spatially variable response of Himalayan glaciers to climate change affected by debris cover. *Nature Geoscience, 4*(3), 156-159. doi: 10.1038/ngeo1068.

Schorghofer, N., & Forget, F. (2012). History and anatomy of subsurface ice on Mars. *Icarus, 220*(2), 1112-1120. doi: 10.1016/j.icarus.2012.07.003.

Séjourné, A., Costard, F., Gargani, J., Soare, R. J., Fedorov, A., & Marmo, C. (2011). Scalloped depressions and small-sized polygons in western Utopia Planitia, Mars: A new formation hypothesis. *Planetary and Space Science, 59*(5–6), 412-422. doi: 10.1016/j.pss.2011.01.007.

Sharp, R. P. (1973). Mars - Fretted and Chaotic Terrains. *Journal of Geophysical Research, 78*(20), 4073-4083. doi: 10.1029/Jb078i020p04073.

Shean, D. E., Head, J. W., & Marchant, D. R. (2005). Origin and evolution of a cold-based tropical mountain glacier on Mars: The Pavonis Mons fan-shaped deposit. *Journal of Geophysical Research-Planets, 110*(E5), E05001. doi: 10.1029/2004je002360.

Sinha, R. K., & Murty, S. V. S. (2013). Evidence of extensive glaciation in Deuteronilus Mensae, Mars: Inferences towards multiple glacial events in the past epochs. *Planetary and Space Science, 86*, 10-32. doi: 10.1016/j.pss.2013.09.002.

Sinha, R. K., & Murty, S. V. S. (2015). Amazonian modification of Moreux crater: Record of recent and episodic glaciation in the Protonilus Mensae region of Mars. *Icarus, 245*, 122-144. doi: 10.1016/j.icarus.2014.09.028.

Smith, M. J. (2011). Chapter Eight - Digital Mapping: Visualisation, Interpretation and Quantification of Landforms. In Smith, M. J., Paron, P. & James, J. S. (Eds.), *Developments in Earth Surface Processes* (Vol. 15, pp. 225-251). Oxford: Elsevier.

Souček, O., Bourgeois, O., Pochat, S., & Guidat, T. (2015). A 3 Ga old polythermal ice sheet in Isidis Planitia, Mars: Dynamics and thermal regime inferred from numerical modeling. *Earth and Planetary Science Letters, 426*, 176-190. doi: 10.1016/j.epsl.2015.06.038.

Souness, C. J., & Hubbard, B. (2013). An alternative interpretation of late Amazonian ice flow: Protonilus Mensae, Mars. *Icarus, 225*(1), 495-505. doi: 10.1016/j.icarus.2013.03.030.

Souness, C. J., Hubbard, B., Milliken, R. E., & Quincey, D. (2012). An inventory and population-scale analysis of martian glacier-like forms. *Icarus, 217*(1), 243-255. doi: 10.1016/j.icarus.2011.10.020.

Squyres, S. W. (1978). Martian Fretted Terrain - Flow of Erosional Debris. *Icarus, 34*(3), 600-613. doi: 10.1016/0019-1035(78)90048-9.

Squyres, S. W. (1979). Distribution of Lobate Debris Aprons and Similar Flows on Mars. *Journal of Geophysical Research, 84*, 8087-8096. doi: 10.1029/Jb084ib14p08087.

Ulrich, M., Morgenstern, A., Günther, F., Reiss, D., Bauch, K. E., Hauber, E., Rössler, S., & Schirrmeister, L. (2010). Thermokarst in Siberian ice-rich permafrost: Comparison to asymmetric scalloped depressions on Mars. *Journal of Geophysical Research: Planets, 115*(E10), E10009. doi: 10.1029/2010je003640.

Van der Veen, C. J. (1999). Fundamentals of Glacier Dynamics. Rotterdam: A. A. Balkema.

Villa, F., De Amicia, M., & Maggi, V. (2007). GIS analysis of Rutor Glacier (Aosta Valley, Italy) volume and terminus variations. *Geografia Fisica e Dinamica Quaternaria, 30*(1), 87-95.

Wolff, I. W., Glasser, N. F., & Hubbard, A. (2013). The reconstruction and climatic implication of an independent palaeo ice cap within the Andean rain shadow east of the former Patagonian ice sheet, Santa Cruz Province, Argentina. *Geomorphology, 185*, 1-15. doi: 10.1016/j.geomorph.2012.10.018.

Zemp, M., Hoelzle, M., & Haeberli, W. (2009). Six decades of glacier mass-balance observations: a review of the worldwide monitoring network. *Annals of Glaciology, 50*(50), 101-111. doi: 10.3189/172756409787769591.

Table 1. Basic descriptive statistics for the environmental parameters of orientation, elevation, relief and latitude for (a) all GLFs (after Souness et al., 2012) and (b) recessional GLFs. See also Figs. S2 and S4 in supplementary material.

| (a) All GLFs	Parameter	Mean	Std. dev.	(b) Recessional GLFs	Parameter	Mean	Std. dev.
All (n = 1293)	Orientation (^{o})	145	117	All (n = 436)	Orientation (^{o})	167	87.0
	Elevation (m)	-363	1950		Elevation (m)	-33	1760
	Relief (m)	364	171		Relief (m)	394	176
	Latitude (^{o})	-	-		Latitude (^{o})	-	-
North (n = 723)	Orientation (^{o})	26	105	North (n = 197)	Orientation (^{o})	49	119
	Elevation (m)	-1370	1290		Elevation (m)	-1170	1180
	Relief (m)	323	161		Relief (m)	340	158
	Latitude (^{o})	39.3	4.90		Latitude (^{o})	38.4	4.80
South (n = 570)	Orientation (^{o})	173	73.0	South (n = 239)	Orientation (^{o})	175	55.0
	Elevation (m)	911	1900		Elevation (m)	900	1600
	Relief (m)	416	169		Relief (m)	439	178
	Latitude (^{o})	-40.8	5.30		Latitude (^{o})	-39.0	3.60
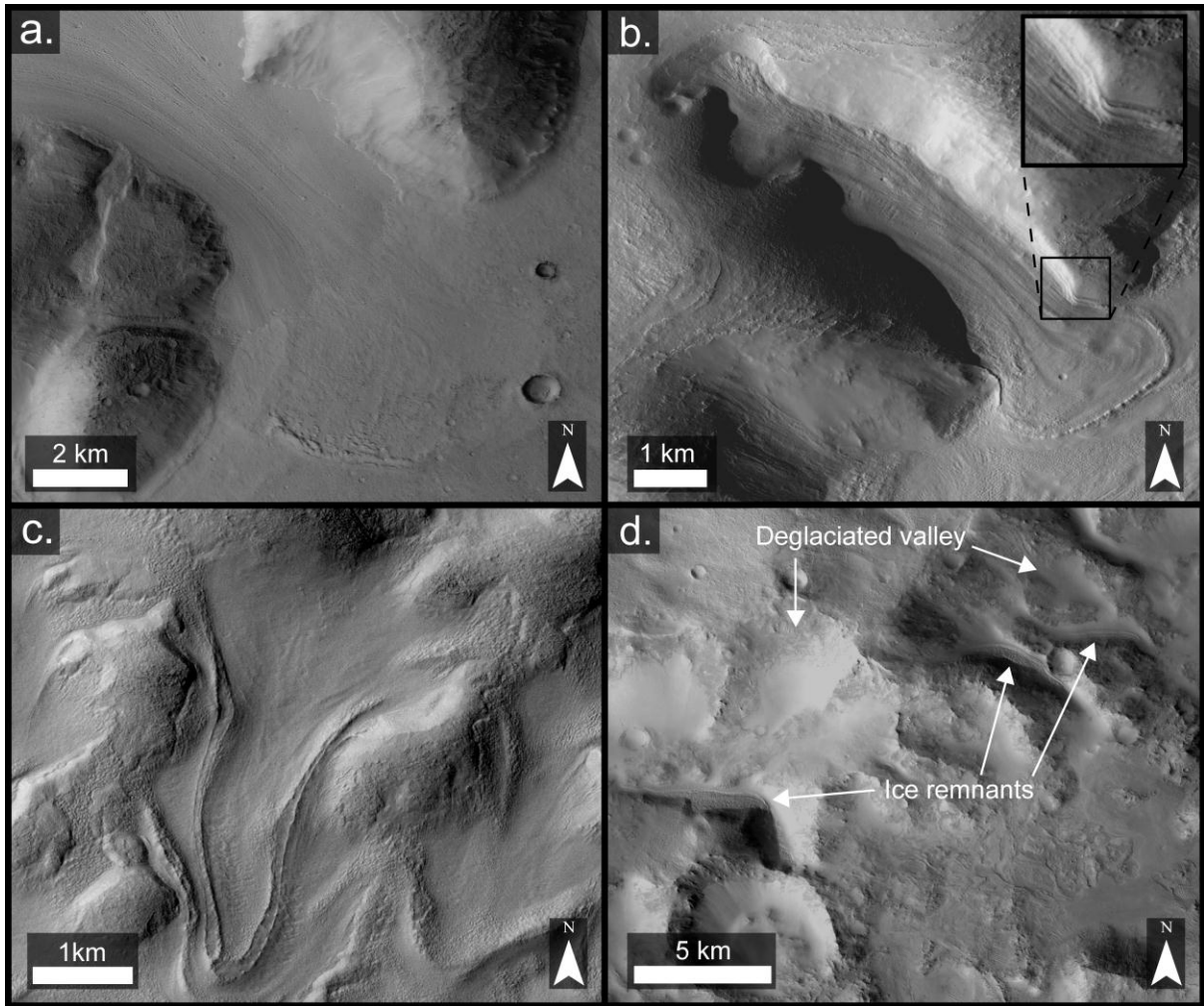
Fig. 1. Montage of CTX images exemplifying GLFs identified as showing evidence of recession. (a) A well-developed set of arcuate moraine ridges demarcating a deglaciated terrain in the foreground of a GLF in Phlegra Montes (subset of CTX image P16_007368_2152_XN_35N195; centred on ~164.54^o E, 34.05^o N). (b) Lateral moraine ridges on eastern sidewall of a GLF in Protonilus Mensae. Note multiple ridges are visible, suggesting progressive or phased recession has occurred (subset of CTX image P01_001570_2213_XI_41N305W; centred on ~54.71^o E, 41.27^o N). (c) Tongue-shaped GLF with pronounced sequence of latero-terminal moraine ridges (subset of CTX image G05_020121_1412_XN_38S247W; centred on ~113.16^o E, 38.15^o S). (d) Palimpsest landscape. Located in close proximity to current GLFs were landscapes indicative of former glaciation. However, as no GLFs are identified in these regions they were not included in the inventory (subset of CTX image P06_003231_2090_XI_29N286W; centred on ~73.15^o E, 30.01^o N).
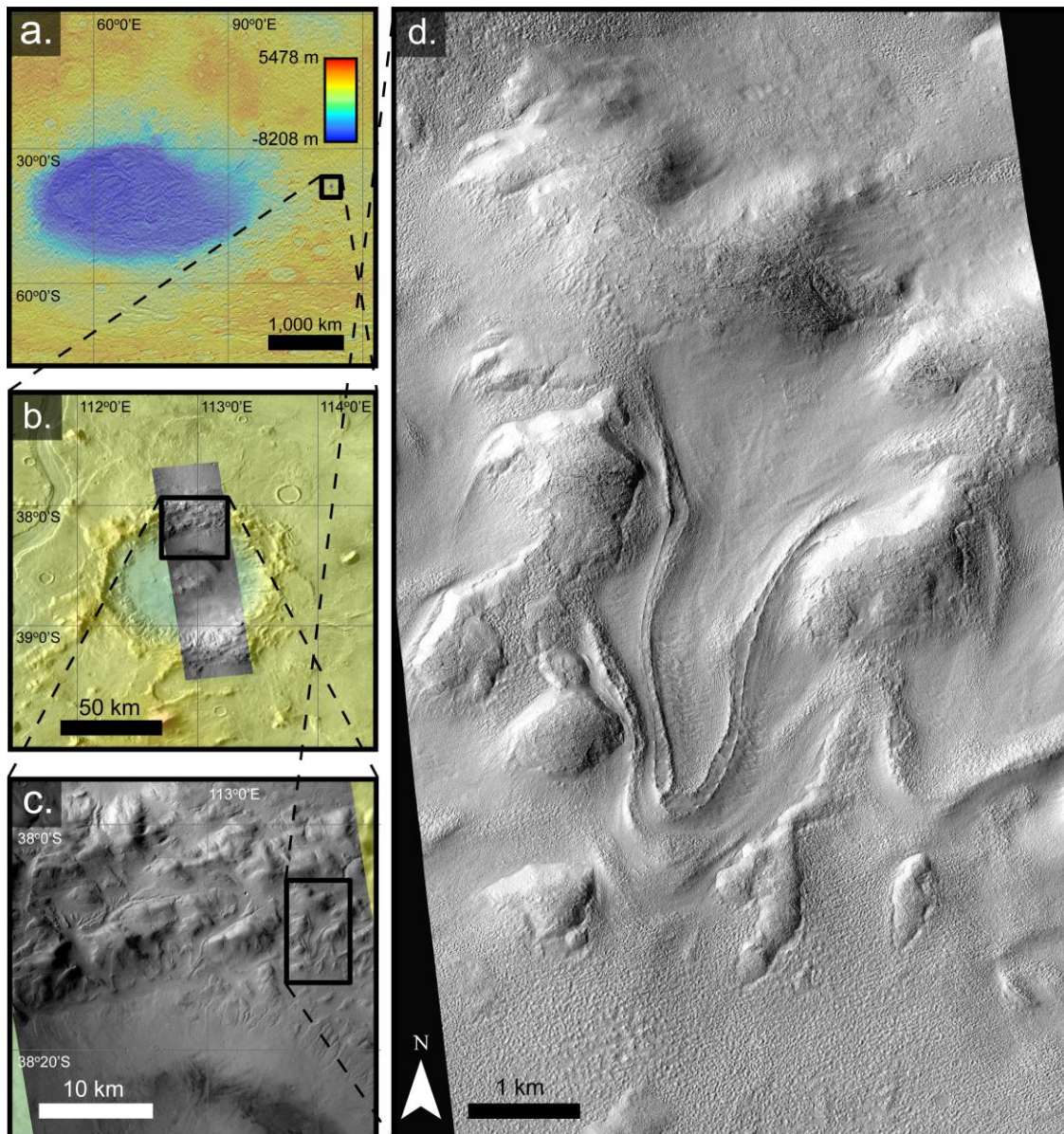
Fig. 2. Location and expansion of our case study GLF reconstruction. (a) Global context map indicating location of host crater, Greg, illustrated as a MOLA elevation transparency overlain on a THEMIS-IR day mosaic. (b, c) Expansion of Crater Greg, illustrating local context and abundance of GLFs on the crater's northern headwall (CTX image G05_020121_1412_XN_38S247W). (d) The subject GLF to reconstruction, illustrated as a subset of HiRISE image PSP_002320_1415_RED (centred on ~113.16° E, 38.15° S).
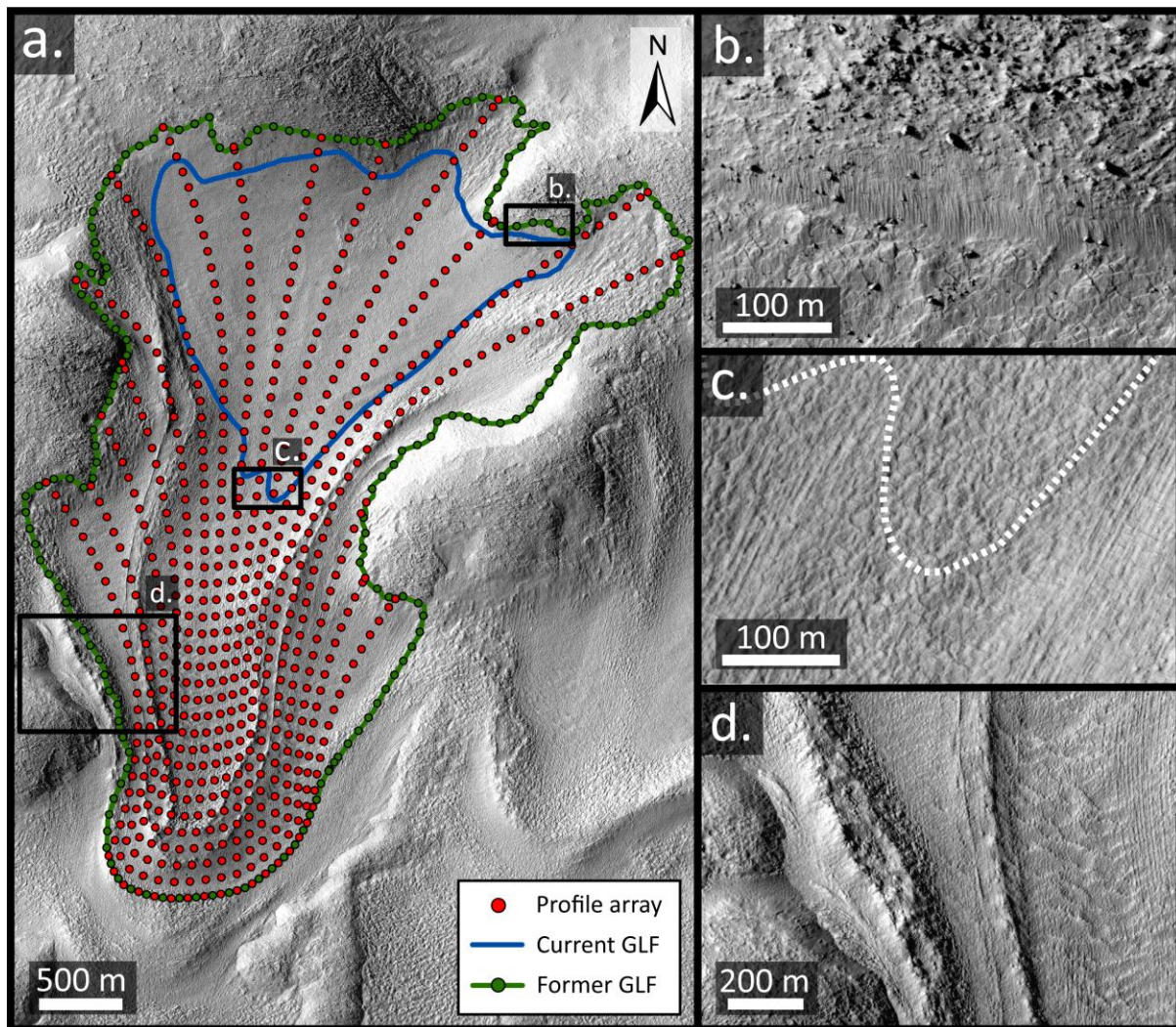
Fig. 3. Interpreted GLF limits and reconstruction array (subset of HiRISE image PSP_002320_1415_RED). (a) Overview of mapped current (blue line) and former (green line) GLF limits with glacier surface (red) and constraining marginal (green) reconstruction nodes overlain. (b–d) Geomorphological and surface evidence used in demarcating the current and former GLF limits: (b) incised headwall terrain, (c) compositional boundary between relatively fresh 'polygonized' terrain and contrasting 'linear' terrain (dashed white line marks the inferred current GLF terminus) and (d) clearly visible moraine ridges.
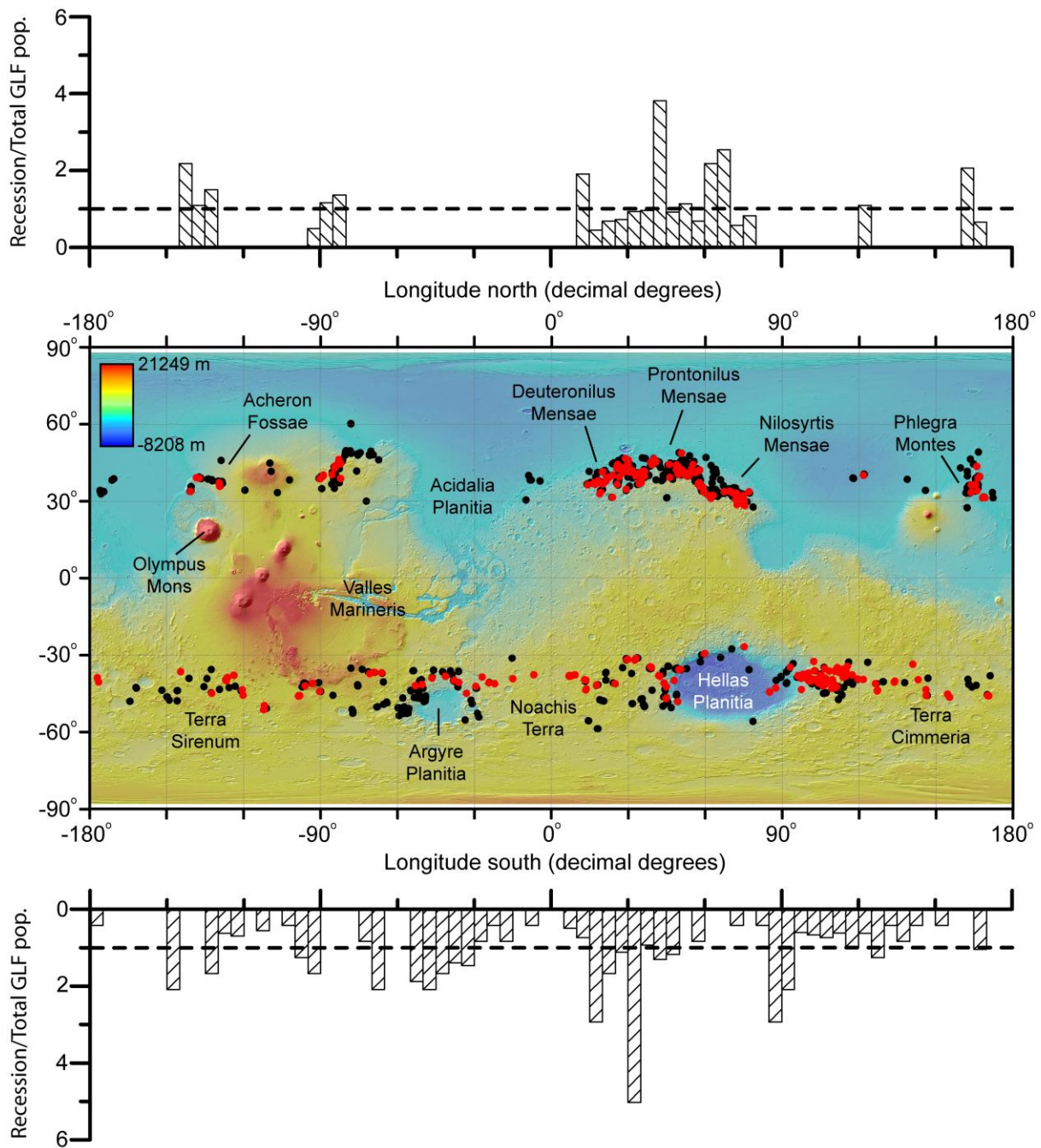
Fig. 4. Mars global map showing the mid-latitude distribution of recessional GLFs (red dots) relative to the total GLF population (black dots). 436 recessional GLFs were identified globally: 197 were located in the northern hemisphere and 239 were located in the southern hemisphere. Ratio bar plots in 5° longitude bins, showing normalised concentration of recessional GLFs relative to the normalised concentration of the total GLF population, for each hemisphere are presented above and below the distribution map. Background map is MOLA elevation transparency overlain on MOLA hillshade projection.
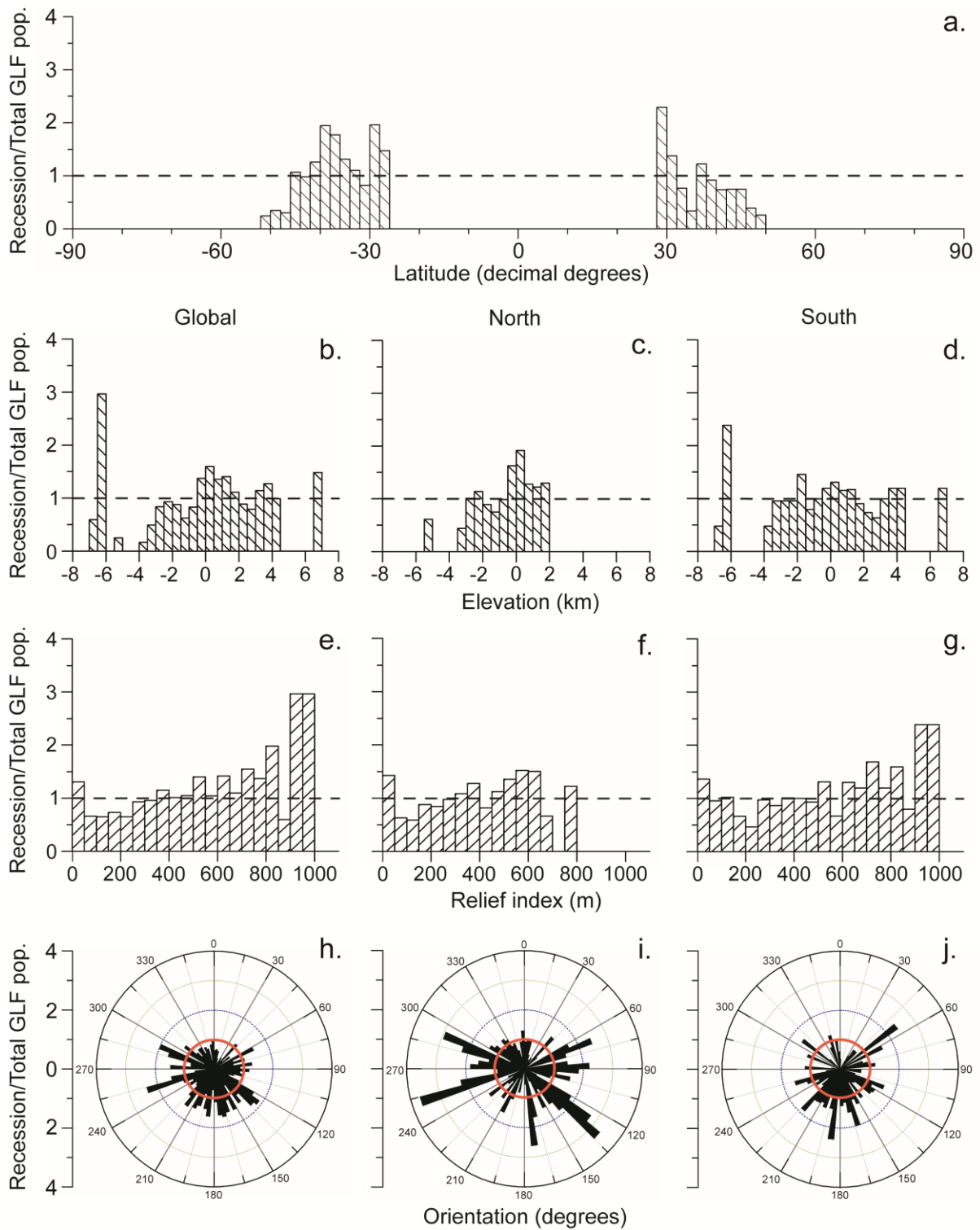
Fig. 5. Ratio plots showing normalised concentration of recessional GLFs relative to the normalised concentration of the total GLF population for: (a) global and hemispheric latitude in 2° bins; (b) global, (c) northern- and (d) southern-hemispheric elevation in 500 m bins; (e) global, (f) northern- and (g) southern-hemispheric relief index in 50 m bins; (h) global, (i) northern- and (j) southern-hemispheric orientation in 5° bins.
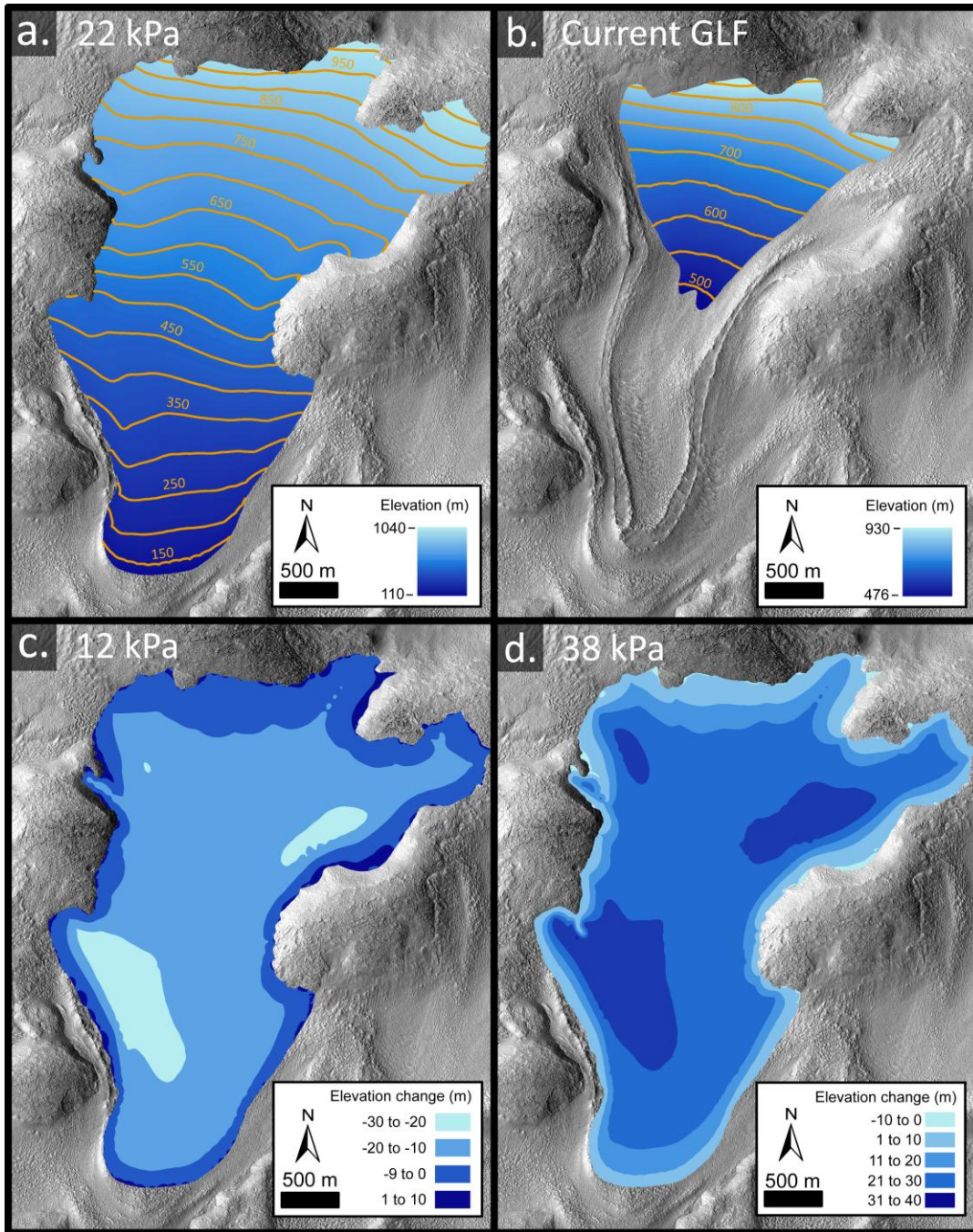
Fig. 6. Crater Greg GLF reconstructed paleo-ice surface. (a) Reconstructed paleo-ice surface based on yield strength of 22 kPa, with 50 m contours. (b) Current ice surface with 50 m contours for comparison. Difference in reconstructed paleo-ice surface from (a) for yield strength of 12 kPa (c) and 38 kPa (d).
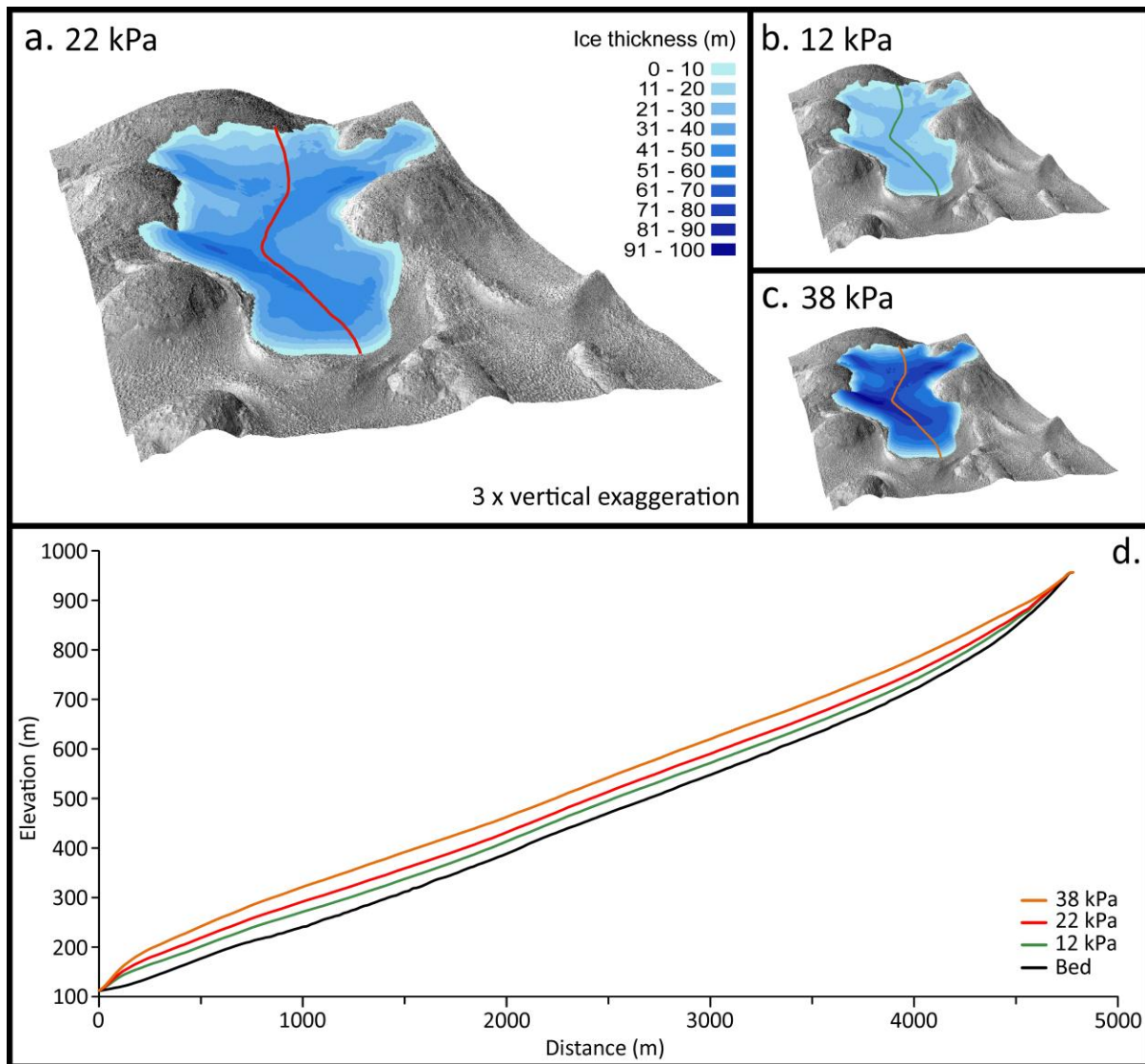
Fig. 7. Crater Greg GLF reconstructed three-dimensional geometry and ice thickness. Reconstructed paleo-ice thickness for yield strength of (a) 22 kPa, (b) 12 kPa and (c) 38 kPa. (d) Paleo-ice surface elevation of (a–c) along a central flow-line.